# The enhanced photoreduction of Cr(VI) to Cr(III) using carbon dots coupled TiO$_2$ mesocrystals

Yaxi Zhang, Mengjiao Xu, Hao Li, Hao Ge, Zhenfeng Bian*

*The Education Ministry Key Laboratory of Resource Chemistry, Shanghai Key Laboratory of Rare Earth Functional Materials, Shanghai Normal University, Shanghai, 200234, PR China*

ABSTRACT

The photocatalytic reduction efficiency of hexavalent chromium (Cr$_2$O$_7^{2-}$ (Cr(VI)) is suffering from high recombination of photoinduced charges, poor adsorption capacity of Cr(VI), and slow desorption of product trivalent chromium (Cr$^{3+}$ (Cr(III))) from photocatalyst surface. In this work, carbon dots (CDs) was coupled with TiO$_2$ mesocrystals (MT), where CDs displayed both the electron collectors and the active sites. During photoreduction of Cr(VI), the as-prepared CD/MT exhibited activity about 5.4 times higher than the pure TiO$_2$ mesocrystals. The positive charges on the CD/MT surface favored the selective adsorption of Cr(VI) and rapid desorption of Cr(III), which has an obvious promotion on the photocatalytic reduction of Cr(VI) and retention of photoreduction activity. Meanwhile, the CDs coupled on TiO$_2$ mesocrystals facilitated the separation of photogenerated charges. This work provides a simple and effective adsorption-photoreduction-desorption mechanism for the photocatalytic reduction of Cr(VI).

## 1. Introduction

Hexavalent chromium (Cr(VI)) was commonly found in the industrial effluents such as electroplating, metal finishing, leather tanning, steel fabricating, photographic, etc [1–4]. It is regarded as one of the most toxic pollutants due to its carcinogenic, mutagenic and teratogenic effects on the biological food chain [1,5,6]. The traditional methods for removing Cr(VI), such as ion exchange, bioremediation, electrodialysis, reduction, membrane separation, adsorption and chemical precipitation [7–13], are limited by the sludge production, incomplete precipitation or high operating costs [14–17]. Photocatalytic reduction of Cr(VI) over TiO$_2$ [18–23], ZnO [24–26], or CdS [27,28], etc. represents a simple, clean and convenient method. Many attempts have been made to enhance the activity by depressing the recombination of photogenerated charges. For example, the deposition of noble metal like Au [29,30], Ag [31,32], and Pt [30,33] nanoparticles on the TiO$_2$ photocatalyst were widely used. Meanwhile, semiconductor heterojunctions have been also widely studied. In addition, one-dimensional CdS@TiO$_2$ core-shell nanocomposites were fabricate, in which TiO$_2$ shell blocked the photogenerated holes from the CdS core [34]. Other cases such as TiO$_2$-boron doped diamond heterojunctions [35] and SnS$_2$/SnO$_2$ nanoheterojunctions [36] have also been developed. Furthermore, sacrificial agents like citric acid has been used to capture the h$^+$ in photoreduction of Cr(VI) on WO$_3$/TiO$_2$ nanotube arrays [37].

Owing to the high toxicity of CdS, SnS$_2$ nanocrystals were synthesized for visible light-driven photocatalytic reduction of Cr(VI), which showed high activity and stability owing to the high adsorption capacity for Cr(VI). However, Cr(III) was found on the surface of SnS$_2$ after fifth recycle, leading to the poison of photocatalyst [38] Both experimental results and theoretical predictions demonstrated that the efficiency for photocatalytic reduction of Cr(VI) to Cr(III) is strongly dependent on the inhibition of photocharge recombination, the high adsorption of Cr(VI) and the rapid desorption of Cr(III) [39]. Therefore, adsorbents such as activated carbon [40,41], graphite oxide [42], metal-organic frameworks [43,44], functionalized CNTs [45] and mesoporous SiO$_2$ [46] are usually combined with photocatalysts to enhance the adsorption of Cr(VI). However, the cooperation between adsorption and photocatalysis sites should be still improved.

Recently, carbon dots (CDs) have been widely used in photocatalysis owing to the excellent photoelectric properties. The surface of CDs has a large number of groups, such as hydroxyl groups and carboxyl groups. These groups have excellent water solubility and suitable chemical reactivity [47,48]. The fluorescence properties of CDs could be adjusted by surface group modification [49,50]. Therefore, we tried to utilize the surface functional groups of CDs as the adsorption sites for capturing Cr(VI). Furthermore, the CDs could capture photoinduced electrons to inhibit their recombination with holes. Therefore, the CDs could be used as both the adsorbent and the photocatalysis promoter. Up to now,

* Corresponding author.
*E-mail addresses:* bianzhenfeng@shnu.edu.cn, bianzhenfeng@163.com (Z. Bian).

CDs has been employed in combining with $C_3N_4$ for hydrogen production [51], with $TiO_2$ for photocatalytic oxidation of organic pollutants [52], and with $Bi_2WO_6$ for photocatalytic oxidation of VOCs [53]. However, CDs have never been used in either adsorption or photocatalytic reduction of Cr(VI). Normally, the size of the CDs is around 5 nm, and it has the characteristics of graphene structure with chemical stability and amorphous shells with tunable oxygen containing groups. Thus, it is expected that the coupling of CDs with $TiO_2$ mesocrystals could inhibit photogenerated charge recombination, leading to the enriched photoelectrons. Besides, the CDs could also promote the adsorption of Cr(VI) and the desorption of Cr(III) by adjusting the surface properties.

Herein, we reported for the first time the CDs coupled $TiO_2$ mesocrystals for photocatalytic reduction of Cr(VI). The $TiO_2$ mesocrystals composed of ordered aligned $TiO_2$ nanocrystal building blocks facilitating the charge transport within the $TiO_2$ superstructure [54,55]. The CDs has a large number of surface oxygen containing groups which can control the adsorption/desorption of Cr(VI)/Cr(III) at a proper range of pH value. On the other hand, the CDs were electron reservoir which were enriched by electrons and thus acted as the reductive sites. The synergistic effect between CDs and $TiO_2$ mesocrystals greatly enhanced photoreduction of Cr(VI).

## 2. Experimental section

### 2.1. Chemicals and materials

$TiOSO_4$ (15 wt% solution in dilute sulfuric acid, purchased from Sigma-Aldrich), $K_2Cr_2O_7$ (Cr(VI), Aldrich), $Cr(NO_3)_3 \cdot 9H_2O$ (Cr(III), Aldrich), ethanol (EtOH, Shanghai Runjie Chemical Reagent Co. Ltd.), *tert*-butyl alcohol, graphite rod (99.99%), diphenylcarbazide (DPC, Aladdin reagent Co. Ltd) were used as received.

### 2.2. Preparation of CDs

CDs were synthesized through an alkali-assisted electrochemical method. In a typical run, the electrolyte in the electrochemical process was prepared by mixing ethanol/$H_2O$ (42 mL; volume ratio = 20:1) with 0.8 g of NaOH. By using graphite rods as both anode and cathode, static potential of 30 V bias was applied to the two electrodes. After 1 h electrolyzing, a black brown solution was obtained. Then, the raw CDs solution was treated by $MgSO_4$ to eliminate the water. Afterwards, the purified CD ethanol solution was obtained by dialysising. The size of CDs is about 2–3 nm (Fig. S1a and c). High-resolution TEM (HRTEM) image showed the detailed structures of CDs (Fig. S1b) which were highly crystallized with the graphite(002) (0.32 nm) crystalline lattices. The CDs sample is a stable ethanol dispersion (Fig. S1d). The CDs sample has the same fluorescence and infrared features consistent with the literature (Fig. S1e and f) [52].

### 2.3. Preparation of $TiO_2$ mesocrystals

$TiO_2$ mesocrystals was prepared from a precursor containing $TiOSO_4$ and *tert*-butyl alcohol (molar ratio = 1:165). The above precursors were transferred into a teflon lined stainless steel autoclave at 110 °C for 48 h. The products were filtered, washed with ethanol, dried at 100 °C and calcined at 350 °C for 2 h, which was named MT [56].

### 2.4. Preparation of CDs/MT

0.3 g $TiO_2$ mixed with different volume (10 mL, 15 mL, 30 mL, 60 mL) of CDs solution and evaporated at 60 °C to obtain CDs/$TiO_2$ mesocrystals composites which were designed as x% CD/MT samples (x and MT represent the mass percentage of CDs and $TiO_2$ mesocrystals).

### 2.5. Characterization of photocatalysts

The samples were characterized using scanning electron microscopy (SEM, HITACHI S4800), transmission electron microscopy (TEM, JEM-2010), X-ray diffraction (XRD, D/MAX-2000 with Cu Kα radiation), Fourier transformation infrared spectrum (FTIR, NEXUS 370), nitrogen sorption (Micromeritics Instrument Corporation, Tristar II 3020, at 77 K) and the surface photovoltage spectrum measurement (lock-in amplifier (SR830) with a light chopper (SR540) and 500 W xenon lamp (LSH-X500)). The Brunauer-Emmett-Teller (BET) method was utilized to calculate the specific surface area. The pore volume and pore diameter distribution were derived from the desorption isotherms by the Barrett-Joyner-Halenda (BJH) model. Fluorescence spectra were measured with the Cary Eclipse Fluorescence Spectrophotometer ($\lambda_{ex}$ = 365 nm). The pH value of Cr ion solution was measured with a pH meter (Mettler Toledo Delta320). Surface electronic states were analyzed by X-ray photoelectron spectroscopy (XPS, PerkinElmer PHI 5000C, Al Kα). All the binding energies were calibrated by using the contaminant carbon ($C_{1S}$ = 284.8 eV) as a reference. Zeta potential of the $TiO_2$ was measured by "Malvern Zetasizer Nano ZS". Photoelectrochemical measurements were performed in a conventional three-electrode, single-compartment quartz cell on an electrochemical station (CHI 660D). A bias voltage of 0.5 V was used to drive the transfer of photogenerated electrons from the working electrode to the platinum electrode. A $Na_2SO_4$ aqueous solution (0.50 M) was used as the electrolyte. Transient absorption spectroscopy was measured using a YAG laser (355 nm, 6 ns full width at half-maximum, 10 mJ/pulse). The reflected analyzing light was from a 500 W Xe lamp. The transient signals were recorded by a digitizer (HP54510B, 300 MHz). All experiments were carried out at room temperature.

### 2.6. Adsorption experiment

In briefly, 20 mg catalyst was added to 20 mL mixture chromium solution (The initial concentration of $Cr_2O_7^{2-}$ ions and $Cr^{3+}$ ions in the mixture solution was 10 mg L$^{-1}$). The mixture was stirred for 0.5 h under the dark condition to reach adsorption–desorption equilibrium. The Cr(VI) concentration was determined by colorimetrically at 540 nm using the diphenylcarbazide method using a UV–vis spectrophotometer (UV 7502/PC) [57]. The amounts of total chromium were determined by inductively coupled plasma (ICP) emission spectroscopy (VISTA-MPX). The concentration of Cr(III) is equal to the total chromium subtracting the Cr(VI) concentration (Cr(III) = $Cr_{total}$-Cr(VI)).

### 2.7. Photocatalytic reduction

For typical photocatalytic runs, 50 mL of $TiO_2$ dispersion (1.0 g/L) containing aqueous solution (Cr(VI), 10 mg/L, pH is about 3 controlled by HCl) using a home-made reactor was stirred for about 30 min to reach adsorption–desorption equilibrium in the dark [54,58]. The photocatalytic reaction was initiated by a LED light (CEL-LED, 365 nm). After stopping the UV illumination, the concentration of Cr(VI) was analyzed by a UV spectrophotometer (UV 7502/PC) at the characteristic wavelength, from which the degradation yield was calculated.

## 3. Results and discussions

SEM images displayed uniform microspheres with average diameter around 600 nm (Fig. 1a). The attached Selected-area electron diffraction (SAED) pattern displayed typical single crystal anatase along the [001] zone axis due to ordered stacking superstructure of secondary nanocrystals (inset of Fig. 1a). Loading CDs had no apparent effect on the morphology (Figs. Figure 1b, c and S2). Highly dispersed CDs were deposited on the surface of $TiO_2$ mesocrystals as shown in the high-resolution TEM (HRTEM) image (Fig. 1d). The size of the CDs is about 2–3 nm and mostly inside the $TiO_2$ cavities. After CDs deposition, the
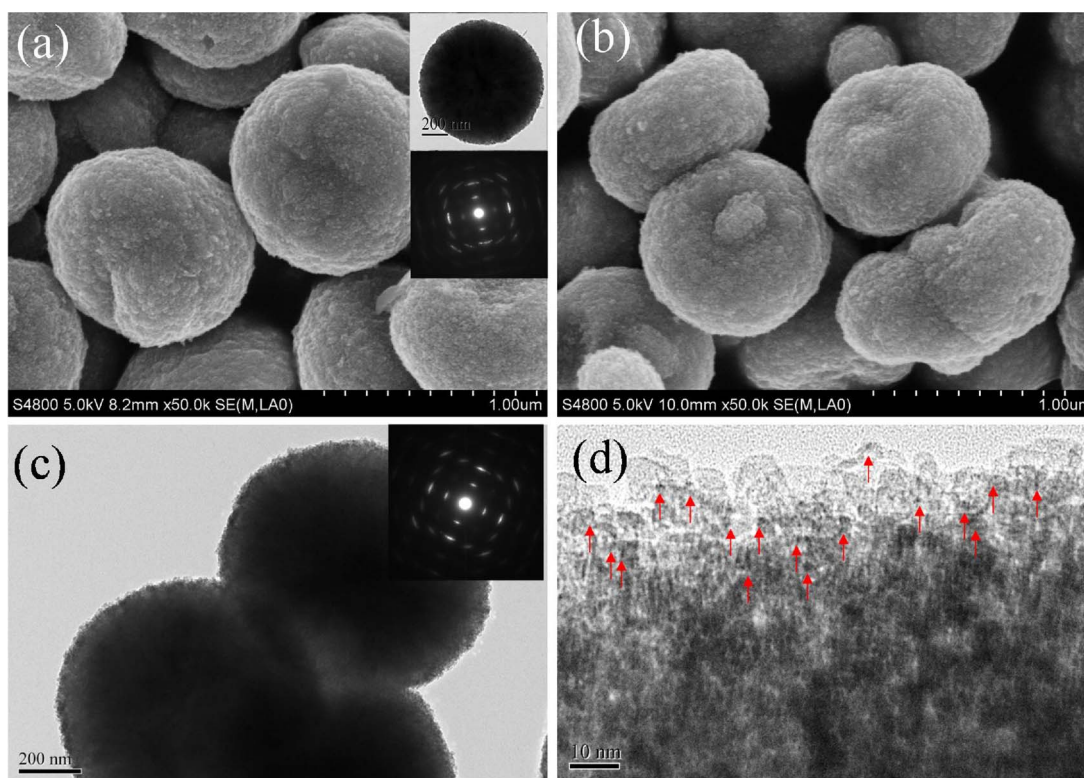
**Fig. 1.** SEM image of (a) MT (insets are the TEM image and SAED pattern recorded on the sample particle) and (b) 0.75 wt% CD/MT, (c) TEM image (inset is the SAED pattern recorded on the sample particle) and (d) HRTEM image of 0.75 wt% CD/MT (The red arrow indicates the position of the CD). (For interpretation of the references to colour in this figure legend, the reader is referred to the web version of this article.)

optical photograph of samples reveal the color change from white to light yellow (Fig. S3), which also indicated the coupling of CDs on $TiO_2$ mesocrystals. Wide-angle X-ray diffraction (XRD) analysis reveals that $TiO_2$ mesocrystals possess typical diffraction peaks of anatase (JCPDS 21-1272) [58,59] and the negligible effect on the crystal structure and crystallinity by coupling with CDs (Fig. S4).

As shown in Fig. 2, all the CD/MT samples including pure MT displayed type II $N_2$ adsorption-desorption isotherms. Based on the calculation from $N_2$ adsorption-desorption isotherms, the surface area values ($S_{BET}$), pore volume ($V_p$), and pore diameter were slightly decreased with the increase of amount of CDs. In comparison with pure $TiO_2$ mesocrystals, The specific surface area ($S_{BET}$) of 0.75 wt% CD/MT was decreased from 109 to 85 $m^2 g^{-1}$, as well as $V_p$ reduced from 0.091 to 0.037 $cm^3 g^{-1}$, while the pore size distribution decreased from 3.7 nm to 3.1 nm (Fig. 2 and Table S1). By further increasing the

amount of CDs, the $S_{BET}$ of 1.5 wt% CD/MT was sharply decreased to 67 $m^2 g^{-1}$, and the $V_p$ reduced to 0.031 $cm^3 g^{-1}$, while the pore size distribution decreased to 2.8 nm. This might be caused by the overloading of CDs caused the blockage of pores in $TiO_2$ mesocrystals.

Fig. 3a revealed that the Cr(VI) reduction efficiency increased from 70% on pure $TiO_2$ mesocrystals to 100% on 0.75 wt% CD/MT after 30 min of UV irradiation. The kinetic studies demonstrated that the Cr(VI) reduction followed a pseudo-first-order reaction expression with a simplified Langmuir−Hinshelwood model. (Fig. 3b). According to the calculated rate constants, the reaction rate of 0.75 wt% CD/MT was about 5.4 times higher than the pure $TiO_2$ mesocrystals. Fig. 4 exhibited more positive zeta potential after coupling $TiO_2$ mesocrystals with CDs, which could be ascribed to the presence of hydroxyl groups on CDs surface, leading to the enhancement of the surface positive charges. To our surprise, the increase of the CDs loading to 1.50 wt% caused
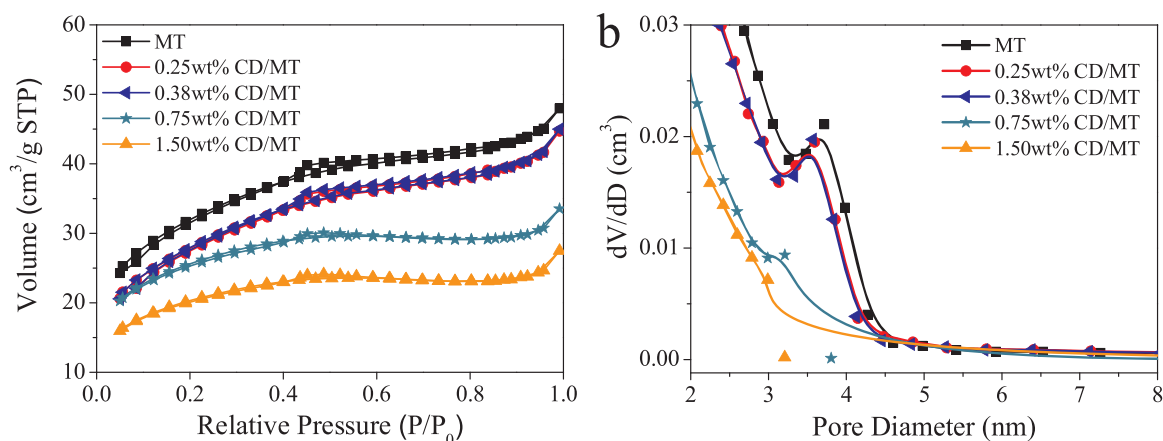


**Fig. 2.** $N_2$ adsorption-desorption isotherms (a) and pore size distribution curves (b) of MT and different CD/MT samples.
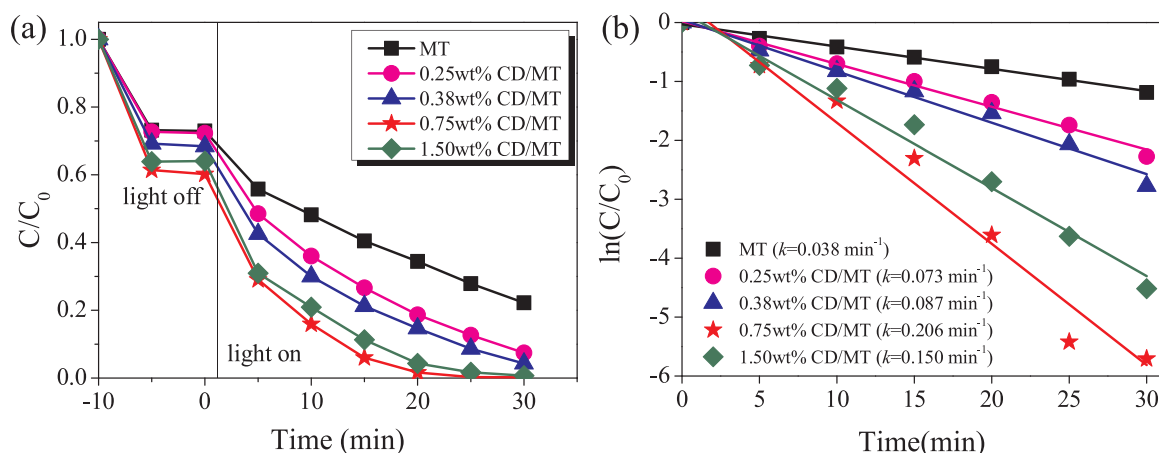
**Fig. 3.** Liquid-phase photocatalytic Cr(VI) anion reduction (a) and kinetic linear fitting curves (b) on different $TiO_2$ samples. (pH = 3.0; $\ln(C_0/C_t) = kt$, where $C_t$ is the concentration of organics at time t, and $k$ is the apparent first-order rate constant.) [30].
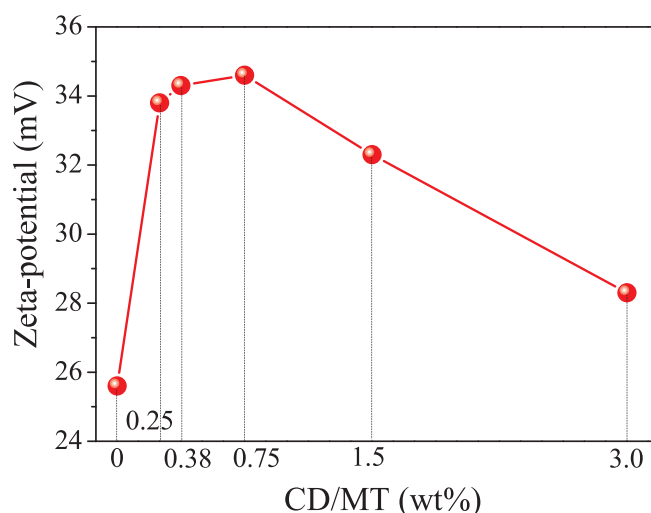


**Fig. 4.** Zeta potentials of MT and different CD/MT samples (pH = 3.0).



**Fig. 5.** Adsorption capacities for Cr(VI)/Cr(III) on different CD/MT samples in a mixed solution containing Cr(VI) and Cr(III).

remarkable decrease of surface charge to 32.3 mV and 3.0 wt% decreased to 28.3 mV. This abnormal phenomenon was caused by the aggregation of CDs, corresponding to the rapid decrease of surface hydroxyl groups, which was consistent with the above $N_2$ adsorption-desorption isotherms. The 0.75 wt% CD/MT exhibited the highest activity in photocatalytic reduction of Cr(VI) since the positive charges on the catalyst surface supplied a large amount of adsorption sites for Cr(VI) anion and the rapid desorption of Cr(III) cation.

In order to investigate the adsorption and repulsion of Cr(VI) and Cr(III) respectively, The adsorption measurement was performed on different x% CD/MT composites. With increasing the loading amounts of CDs on the surface of $TiO_2$ mesocrystals, the adsorption of Cr(III) decreased while the adsorption amount of Cr(VI) increased gradually. The sample of 0.75 wt% CD/MT showed obvious priority for Cr(VI) adsorption (12.0 mg/g), but the adsorption capacity of Cr(III) was very limited (0.8 mg/g) (Fig. 5). The ratio of Cr(VI)/Cr(III) adsorption capacity increased from 7.1 of pure $TiO_2$ mesocrystals to 15 of 0.75 wt% CD/MT composite (Table S1), which confirmed that the CDs coupling on the $TiO_2$ mesocrystals promoted Cr(VI) adsorption and facilitated Cr(III) desorption owing to positive surface charges, leading to the enhanced activity in photocatalytic reduction of Cr(VI) to Cr(III). As expected, the 1.50 and 3.0 wt% CD/MT showed a decreased ratio between Cr(VI) and Cr(III) adsorption capacities due to the decreased surface zeta potential. Therefore, the important thing is that the Zeta-potential affects the adsorption capacities of CD/MT samples.
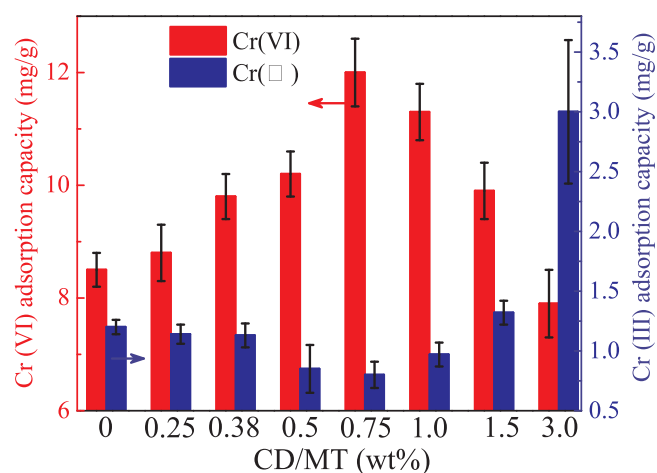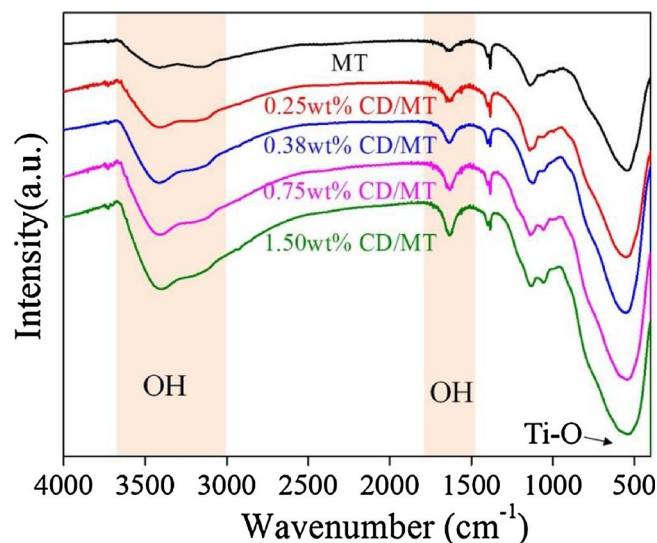


**Fig. 6.** FTIR spectra of the different CD/MT samples.

FTIR spectra (Fig. 6) has been employed to detect the hydroxyl groups on $TiO_2$ surface. A broad stretching vibration near 3400 $cm^{-1}$ and another peak around 1630 $cm^{-1}$ can be attributed to the surface-adsorbed water and hydroxyl groups [22], respectively, which become
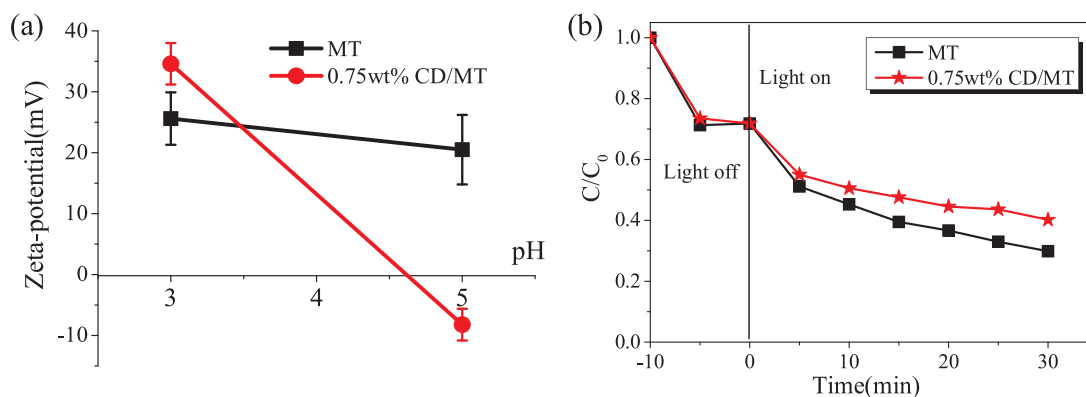
**Fig. 7.** (a) Zeta potentials and (b) Liquid-phase photocatalytic Cr(VI) anion reduction of MT and 0.75 wt% CD/MT sample (pH = 5.0).
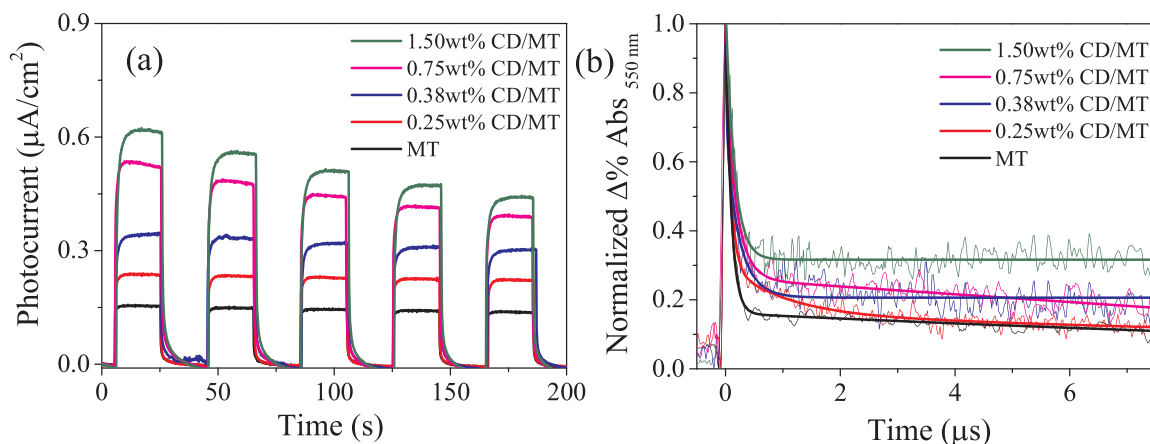


**Fig. 8.** (a) Photocurrent responses of different TiO2 samples under UV light irradiation. (b) Differential time traces of%Abs at 550 nm obtained from different MT sample.
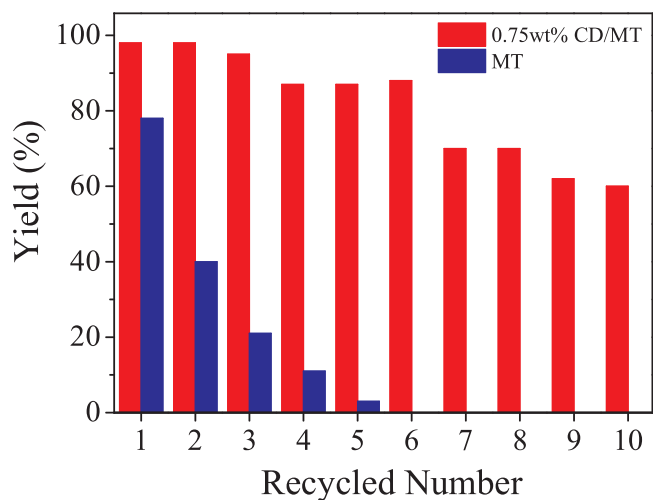


**Fig. 9.** Recycling tests of the MT and 0.75 wt% CD/MT sample. (pH = 3.0).

more obvious after CDs loading. XPS was also used to investigate the amount of surface hydroxyl groups [60]. The O1s peak is fitting by pseudo-Voigt functions. The O1s signal shows three peaks at 530.1, 531.7 and 532.9 eV (Fig. S5). The main peak at 530.1 eV could be ascribed to lattice oxygen in TiO2, as well as the signal at 531.7 eV could be associated to surface hydroxyl groups, while the peak at 532.9 eV might be adsorbed H2O. From the results, it can be seen that the number of surface hydroxyl groups on TiO2 are significantly improved after CD loading. However, the surface hydroxyl groups on 1.50 wt% CD/MT slightly decreased.

Zeta-potential of MT and 0.75 wt% CD/MT were also measured at different pH values (Fig. 7a). The zeta-potential value was 34.6 mV for the 0.75 wt% CD/MT sample which was higher than the pure TiO2 mesocrystals (25.6 mV) at pH of 3.0. However, as the pH was 5.0, the zeta-potential value was diametrically changed. The zeta potential value of 0.75 wt% CDs/MT sample was about −8.2 mV, while pure TiO2 mesocrystals was about 20.5 mV. The photoreduction activity of 0.75 wt% CDs/MT was only achieved 65% of pure TiO2 mesocrystals at pH of 5 (Figs. Figure 7b and S6). Those results further demonstrated that the selective adsorption-desorption of Cr(VI) and Cr(III) played a key role in determining the photocatalytic reduction performance. It is mainly due to the modification of CDs. Zeta-potential value of pure CDs were changed at pH 3 and 5 (Fig. S7). A more positive charge surface was beneficial to the Cr(VI) absorption and Cr(III) desorption in the photocatalytic reduction of Cr(VI) to Cr(III).

The separation efficiency of photo-exited charges (e/h pair) and the enrichment of electrons on the surface of CDs were investigated by the photocurrent under UV light irradiation. As shown in Fig. 8a, the photocurrent generated on CDs/MT samples is significantly enhanced after CDs loading. The result reflects that the conductive CDs can be more effective for the migration of photogenerated electrons from TiO2 surface to CDs through a conductive pathway.

TiO2 exhibits a broad transient absorption peak in the visible to near-infrared range under 355 nm laser excitation, which represents the overlapping of the trapped holes (about 440–600 nm) and trapped electrons (about 660–900 nm) [54,55]. Transient absorption spectroscopy was employed to measure the lifetime of a charge-separated state. The absorption data of the 550 nm absorption should be used to determine the rate of charge recombination in TiO2. As shown in Fig. 8b, the lifetime of photogenerated charges of 1.50 wt% CD/MT is much
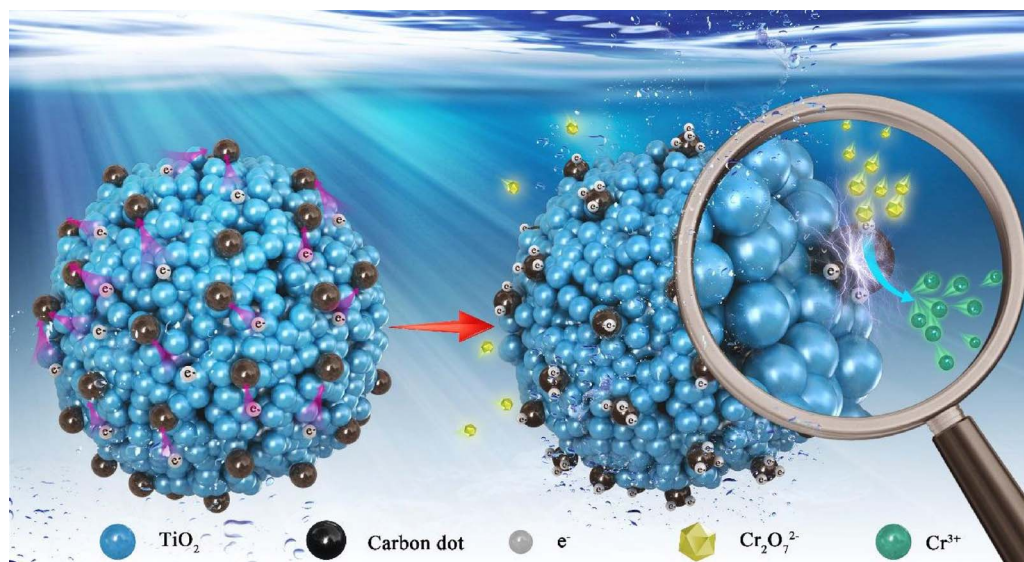
**Fig. 10.** A proposed adsorption-photo-reduction-desorption mechanisms of photocatalytic reduction of Cr(VI) in the presence of CDs/MT composite.

longer than that of MT, 0.25 wt% CD/MT, 0.38 wt% CD/MT and 0.75 wt% CD/MT. The results are in good agreement with the photocurrent, indicating that the CDs loading facilitating the separation of photoinduced charge.

As shown in Fig. 9, 0.75 wt% CDs/MT retained 60% yield after 10 times photocatalytic reduction of Cr(VI), while the pure TiO$_2$ mesocrystals retained only 3% (almost inactivation) yield after 5 times reaction. The main reason for the deactivation of pure TiO$_2$ mesocrystals is the deposition of Cr(III) on the reactive sites of TiO$_2$ surface. The relative higher durability and stability of 0.75 wt% CDs/MT composite was attributed to the positive surface, which is benefit to remove Cr(III) cation during the photocatalytic reduction process. Furthermore, the activity of 0.75 wt% CDs/MT sample decreased after 7 cycles. The reason for the decreased activity might be the surface active sites covered by photocatalytic reduction products (Cr(III)). Although the surface has the ability of selective desorption of Cr(III), there must be a small amount of Cr(III) residues at the surface active sites. After repeated 7 cycles, the Cr(III) content on the surface gradually increases, which affects the photocatalytic performance. XPS results were used to investigate the Cr(III) on the surface of the sample. As shown in Fig. S8, the binding energy of Cr 2p3/2 was observed at 576.83 eV which corresponded to Cr(III).

Based on the above results, we proposed the adsorption-photoreduction-desorption mechanisms (Fig. 10). CDs were coupled with TiO$_2$ mesocrystals with high porosity and surface oxygen containing groups, which endowed TiO$_2$ with positively charged surface. CDs with high stability and good conductivity improved the separation efficiency of photogenerated charges. Accordingly, the positive charged photocatalyst facilitated the adsorption of Cr(VI) and the desorption of Cr(III) during the process of photocatalytic reduction of Cr(VI). Herein, CDs on TiO$_2$ mesocrystals acted as both the adsorption sites for Cr(VI) and the active sites for the photocatalytic reduction of Cr(VI). The rapid desorption of product Cr(III) on the CD/MT catalyst enhanced both the activity and the durability in the during photocatalytic reduction of Cr(VI) to Cr(III).

## 4. Conclusion

In summary, CDs coupled TiO$_2$ mesocrystals photocatalysts showed obvious enhanced photocatalytic reduction activity of Cr(VI). There are three main roles of CDs: 1. CDs improved the separation efficiency of photogenerated charges on TiO$_2$; 2. CDs as electron collectors for enriching electrons; 3. CDs endowed the TiO$_2$ with the more positive charged surface. The photoreduction rate of CD/MT composite reached about 5.4 times higher activity compared with pure TiO$_2$ mesocrystals when pH was 3.0. The CDs/MT composite has the relative higher durability and stability during the photocatalytic reduction process. We proposed an adsorption-photoreduction-desorption mechanism to illustrate the enhanced photocatalytic reduction performance of the CD/MT composites.

## Acknowledgments

## Appendix A. Supplementary data

Supplementary data associated with this article can be found, in the online version, at https://doi.org/10.1016/j.apcatb.2017.12.053.

## References

[1] D. Blowes, Tracking hexavalent Cr in groundwater, Science 295 (2002) 2024–2025.
[2] E. Vaiopoulou, P. Gikas, Effects of chromium on activated sludge and on the performance of wastewater treatment plants: a review, Water Res. 246 (2012) 549–570.
[3] M. Costa, Potential hazards of hexavalent chromate in our drinking water, Toxicol. Appl. Pharmacol. 188 (2003) 1–5.
[4] L. Hsu, S. Wang, Y. Lin, M. Wang, P. Chiang, J. Liu, W. Kuan, C. Chen, Y. Tzou, Cr (VI) removal on fungal biomass of Neurospora crassa: the importance of dissolved organic carbons derived from the biomass to Cr(VI) reduction, Environ. Sci. Technol. 44 (2010) 6202–6208.
[5] A. Linos, A. Petralias, C.A. Christophi, E. Christoforidou, P. Kouroutou, M. Stoltidis, A. Veloudaki, E. Tzala, K.C. Makris, M.R. Karagas, Oral ingestion of hexavalent chromium through drinking water and cancer mortality in an industrial area of Greece-An ecological study, Environ. Health 10 (2011) 50–57.
[6] A. Zhitkovich, Chromium in drinking water: sources, metabolism, and cancer risks, Chem. Res. Toxicol. 24 (2011) 1617–1629.
[7] D. Aggarwal, M. Goyal, R. Bansal, Adsorption of chromium by activated carbon from aqueous solution, Carbon 37 (1999) 1989–1997.
[8] C.E. Barrera-Diaz, V. Lugo-Lugo, B. Bilyeu, A review of chemical electrochemical and biological methods for aqueous Cr(VI) reduction, J. Hazard. Mater. 223–224 (2012) 1–12.
[9] A. Bhattacharya, T. Naiya, S. Mandal, S. Das, Adsorption, kinetics and equilibrium studies on removal of Cr(VI) from aqueous solutions using different low-cost adsorbents, Chem. Eng. J. 137 (2008) 529–541.

[10] Q. Chen, Z. Luo, C. Hills, G. Xue, M. Tyrer, Precipitation of heavy metals from wastewater using simulated flue gas: sequent additions of fly ash, lime and carbon dioxide, Water Res. 43 (2009) 2605–2614.

[11] I. Ortiz, M.F. San Roman, S.M. Corvalan, A.M. Eliceche, Modeling and optimization of an emulsion pertraction process for removal and concentration of Cr (VI), Ind. Eng. Chem. Res. 42 (2003) 5891–5899.

[12] Y. Sharma, C. Weng, Removal of chromium (VI) from water and wastewater by using riverbed sand: kinetic and equilibrium studies, J. Hazard. Mater. 142 (2007) 449–454.

[13] N. Wu, H. Wei, L. Zhang, Efficient removal of heavy metal ions with biopolymer template synthesized mesoporous titania beads of hundreds of micrometers size, Environ. Sci. Technol. 46 (2012) 419–425.

[14] J. Hu, I.M. Lo, G. Chen, Fast removal and recovery of Cr(VI) using surface-modified jacobsite (MnFe$_2$O$_4$) nanoparticles, Langmuir 21 (2005) 11173–11179.

[15] Y.C. Zhang, J. Li, H.Y. Xu, One-step in situ solvothermal synthesis of SnS$_2$/TiO$_2$ nanocomposites with high performance in visible light-driven photocatalytic reduction of aqueous Cr(VI), Appl. Catal. B 123 (2012) 18–26.

[16] R. Güell, E. Anticó, V. Salvadó, C. Fontàs, Efficient hollow fiber supported liquid membrane system for the removal and preconcentration of Cr(VI) at trace levels, Sep. Purif. Technol. 62 (2008) 389–393.

[17] D. Mohan, C.U. Pittman, Activated carbons and low cost adsorbents for remediation of tri-and hexavalent chromium from water, J. Hazard. Mater. 137 (2006) 762–811.

[18] B. Sun, E.P. Reddy, P.G. Smirniotis, Visible light Cr(VI) reduction and organic chemical oxidation by TiO$_2$ photocatalysis, Environ. Sci. Technol. 39 (2005) 6251–6259.

[19] H. Park, H.-I. Kim, G.-h. Moon, W. Choi, Photoinduced charge transfer processes in solar photocatalysis based on modified TiO$_2$, Energy Environ. Sci. 9 (2016) 411–433.

[20] L. Wang, N. Wang, L. Zhu, H. Yu, H. Tang, Photocatalytic reduction of Cr(VI) over different TiO$_2$ photocatalysts and the effects of dissolved organic species, J. Hazard. Mater. 152 (2008) 93–99.

[21] J.J. Testa, M.A. Grela, M.I. Litter, Heterogeneous photocatalytic reduction of chromium (VI) over TiO$_2$ particles in the presence of oxalate: involvement of Cr(V) species, Environ. Sci. Technol. 38 (2004) 1589–1594.

[22] Y. Li, Y. Bian, H. Qin, Y. Zhang, Z. Bian, Photocatalytic reduction behavior of hexavalent chromium on hydroxyl modified titanium dioxide, Appl. Catal. B 206 (2017) 293–299.

[23] H. Qin, Y. Bian, Y. Zhang, L. Liu, Z. Bian, Effect of Ti (III) surface defects on the process of photocatalytic reduction of hexavalent chromium, Chin. J. Chem. 35 (2017) 203–208.

[24] E. Selli, A. De Giorgi, G. Bidoglio, Humic acid-sensitized photoreduction of Cr (VI) on ZnO particles, Environ. Sci. Technol. 30 (1996) 598–604.

[25] Y. Zhang, Z. Chen, S. Liu, Y.-J. Xu, Size effect induced activity enhancement and anti-photocorrosion of reduced graphene oxide/ZnO composites for degradation of organic dyes and reduction of Cr(VI) in water, Appl. Catal. B 140 (2013) 598–607.

[26] X. Liu, L. Pan, Q. Zhao, T. Lv, G. Zhu, T. Chen, T. Lu, Z. Sun, C. Sun, UV-assisted photocatalytic synthesis of ZnO–reduced graphene oxide composites with enhanced photocatalytic activity in reduction of Cr(VI), Chem. Eng. J. 183 (2012) 238–243.

[27] X. Liu, L. Pan, T. Lv, G. Zhu, Z. Sun, C. Sun, Microwave-assisted synthesis of CdS-reduced graphene oxide composites for photocatalytic reduction of Cr(VI), Chem. Commun. 47 (2011) 11984–11986.

[28] N. Nasrallah, M. Kebir, Z. Koudri, M. Trari, Photocatalytic reduction of Cr(VI) on the novel hetero-system CuFe$_2$O$_4$/CdS, J. Hazard. Mater. 185 (2011) 1398–1404.

[29] Z. Bian, T. Tachikawa, P. Zhang, M. Fujitsuka, T. Majima, Au/TiO$_2$ superstructure-based plasmonic photocatalysts exhibiting efficient charge separation and unprecedented activity, J. Am. Chem. Soc. 136 (2014) 458–465.

[30] Z. Bian, T. Tachikawa, W. Kim, W. Choi, T. Majima, Superior electron transport and photocatalytic abilities of metal-nanoparticle-loaded TiO$_2$ superstructures, J. Phys. Chem. C 116 (2016) 25444–25453.

[31] Y. Choi, M.S. Koo, A.D. Bokare, D.H. Kim, D.W. Bahnemann, W. Choi, Sequential process combination of photocatalytic oxidation and dark reduction for the removal of organic pollutants and Cr(VI) using Ag/TiO$_2$, Environ. Sci. Technol. 51 (2017) 3973–3981.

[32] A. Takai, P.V. Kamat, Capture, store, and discharge. Shuttling photogenerated electrons across TiO$_2$–silver interface, ACS Nano 5 (2011) 7369–7376.

[33] X. Pan, Y.-J. Xu, Defect-mediated growth of noble-metal (Ag Pt, and Pd) nanoparticles on TiO$_2$ with oxygen vacancies for photocatalytic redox reactions under visible light, J. Phys. Chem. C 117 (2013) 17996–18005.

[34] S. Liu, N. Zhang, Z.R. Tang, Y.J. Xu, Synthesis of one-dimensional CdS@TiO$_2$ core-shell nanocomposites photocatalyst for selective redox: the dual role of TiO$_2$ shell, ACS Appl. Mater. Interfaces 4 (2012) 6378–6385.

[35] H. Yu, S. Chen, X. Quan, H. Zhao, Y. Zhang, Fabrication of a TiO$_2$- BDD heterojunction and its application as a photocatalyst for the simultaneous oxidation of an

Azo dye and reduction of Cr (VI), Environ. Sci. Technol. 42 (2008) 3791–3796.

[36] Y.C. Zhang, L. Yao, G. Zhang, D.D. Dionysiou, J. Li, X. Du, One-step hydrothermal synthesis of high-performance visible-light-driven SnS$_2$/SnO$_2$ nanoheterojunction photocatalyst for the reduction of aqueous Cr(VI), Appl. Catal. B 144 (2014) 730–738.

[37] L. Yang, Y. Xiao, S. Liu, Y. Li, Q. Cai, S. Luo, G. Zeng, Photocatalytic reduction of Cr (VI) on WO$_3$ doped long TiO$_2$ nanotube arrays in the presence of citric acid, Appl. Catal. B 94 (2010) 142–149.

[38] Y.C. Zhang, J. Li, M. Zhang, D.D. Dionysiou, Size-tunable hydrothermal synthesis of SnS$_2$ nanocrystals with high performance in visible light-driven photocatalytic reduction of aqueous Cr(VI), Environ. Sci. Technol. 45 (2011) 9324–9331.

[39] A. Kubacka, M. Fernandez-Garcia, G. Colon, Advanced nanoarchitectures for solar photocatalytic applications, Chem. Rev. 112 (2012) 1555–1614.

[40] T. Karthikeyan, S. Rajgopal, L.R. Miranda, Chromium(VI) adsorption from aqueous solution by Hevea Brasilinesis sawdust activated carbon, J. Hazard. Mater. 124 (2005) 192–199.

[41] K. Selvi, S. Pattabhi, K. Kadirvelu, Removal of Cr(VI) from aqueous solution by adsorption onto activated carbon, Bioresour. Technol. 80 (2001) 87–89.

[42] H. Jabeen, V. Chandra, S. Jung, J.W. Lee, K.S. Kim, S.B. Kim, Enhanced Cr(VI) removal using iron nanoparticle decorated graphene, Nanoscale 3 (2011) 3583–3585.

[43] X. Li, X. Gao, L. Ai, J. Jiang, Mechanistic insight into the interaction and adsorption of Cr(VI) with zeolitic imidazolate framework-67 microcrystals from aqueous solution, Chem. Eng. J. 274 (2015) 238–246.

[44] L. Aboutorabi, A. Morsali, E. Tahmasebi, O. Buyukgungor, Metal-organic framework based on isonicotinate N-oxide for fast and highly efficient aqueous phase Cr (VI) adsorption, Inorg. Chem. 55 (2016) 5507–5513.

[45] N. Shaham Waldmann, Y. Paz, Photocatalytic reduction of Cr (VI) by titanium dioxide coupled to functionalized CNTs: an example of counterproductive charge separation, J. Phys. Chem. C 114 (2010) 18946–18952.

[46] N. Li, F. Fu, J. Lu, Z. Ding, B. Tang, J. Pang, Facile preparation of magnetic mesoporous MnFe$_2$O$_4$@SiO$_2$-CTAB composites for Cr(VI) adsorption and reduction, Environ. Pollut. 220 (2016) 1376–1385.

[47] L.-W. Zhang, H.-B. Fu, Y.-F. Zhu, Efficient TiO$_2$ photocatalysts from surface hybridization of TiO$_2$ particles with graphite-like carbon, Adv. Funct. Mater. 18 (2008) 2180–2189.

[48] H. Li, Z. Kang, Y. Liu, S.-T. Lee, Carbon nanodots: synthesis, properties and applications, J. Mater. Chem. 22 (2012) 24230–24252.

[49] S.N. Baker, G.A. Baker, Luminescent carbon nanodots: emergent nanolights, Angew. Chem. Int. Ed. 49 (2010) 6726–6744.

[50] X.T. Zheng, A. Ananthanarayanan, K.Q. Luo, P. Chen, Glowing graphene quantum dots and carbon dots: properties, syntheses, and biological applications, Small 11 (2015) 1620–1636.

[51] J. Liu, Y. Liu, N. Liu, Y. Han, X. Zhang, H. Huang, Y. Lifshitz, S.-T. Lee, J. Zhong, Z. Kang, Metal-free efficient photocatalyst for stable visible water splitting via a two-electron pathway, Science 347 (2015) 970–974.

[52] H. Ming, Z. Ma, Y. Liu, K. Pan, H. Yu, F. Wang, Z. Kang, Large scale electrochemical synthesis of high quality carbon nanodots and their photocatalytic property, Dalton Trans. 41 (2012) 9526–9531.

[53] X. Qian, D. Yue, Z. Tian, M. Reng, Y. Zhu, M. Kan, T. Zhang, Y. Zhao, Carbon quantum dots decorated Bi$_2$WO$_6$ nanocomposite with enhanced photocatalytic oxidation activity for VOCs, Appl. Catal. 193 (2016) 16–21.

[54] Z. Bian, T. Tachikawa, T. Majima, Superstructure of TiO$_2$ crystalline nanoparticles yields effective conduction pathways for photogenerated charges, J. Phys. Chem. Lett. 3 (2012) 1422–1427.

[55] F. Chen, F. Cao, H. Li, Z. Bian, Exploring the important role of nanocrystals orientation in TiO$_2$ superstructure on photocatalytic performances, Langmuir 31 (2015) 3494–3499.

[56] Z. Bian, J. Zhu, J. Wen, F. Cao, Y. Huo, X. Qian, Y. Cao, M. Shen, H. Li, Y. Lu, Single-crystal-like titania mesocages, Angew. Chem. Int. Ed. 50 (2011) 1105–1108.

[57] L. Huang, C.H. Yu, P.K. Hopke, P.J. Lioy, B.T. Buckley, J.Y. Shin, Z.T. Fan, Measurement of soluble and total hexavalent chromium in the ambient airborne particles in New Jersey, Aerosol Air Qual. Res. 14 (2014) 1939–1949.

[58] H. Li, Z. Bian, J. Zhu, Y. Huo, H. Li, Y. Lu, Mesoporous Au/TiO$_2$ nanocomposites with enhanced photocatalytic activity, J. Am. Chem. Soc. 129 (2007) 4538–4539.

[59] H. Li, Z. Bian, J. Zhu, D. Zhang, G. Li, Y. Huo, H. Li, Y. Lu, Mesoporous titania spheres with tunable chamber stucture and enhanced photocatalytic activity, J. Am. Chem. Soc. 129 (2007) 8406–8407.

[60] J. Zhu, J. Yang, Z.F. Bian, J. Ren, Y.M. Liu, Y. Cao, H.X. Li, H.Y. He, K.N. Fan, Nanocrystalline anatase TiO$_2$ photocatalysts prepared via a facile low temperature nonhydrolytic sol–gel reaction of TiCl$_4$ and benzyl alcohol, Appl. Catal. B 76 (2007) 82–91.